

Article

# Control of Flow Past a Circular Cylinder Using a Rotating Control Rod

Ming Zhao \*  and Erfan Taheri

School of Engineering, Design and Built Environment, Western Sydney University, Penrith, NSW 2751, Australia; 17783747@student.westernsydney.edu.au

\* Correspondence: m.zhao@westernsydney.edu.au

**Abstract:** Control of flow past a circular cylinder using a rotating control rod is investigated by conducting two-dimensional numerical simulations with a Reynolds number of 200, a rod-to-cylinder diameter ratio of 0.2, a gap ratio of 0.2, position angles of the control rod between  $0^\circ$  and  $180^\circ$ , and rotation rates between  $-7$  and  $7$ . The rotation rate is positive if the cylinder rotates in the anticlockwise direction. The aim of this paper is to discover the effects of the position angle and the rotation rate on flow control. If the rod is placed at the side (position angle =  $90^\circ$ ) or nearly to the side of the cylinder (position angle =  $45^\circ$  and  $135^\circ$ ), the rotating rod affects the flow in three ways, depending on its rotation rate: (1) strong negative rotation of the rod weakens the negative free shear layers and reduces the lift; (2) flow through the gap interferes with vortex shedding when the rotation rate is small in either direction; and (3) strong positive rotation of the rod enhances the negative free shear layers and increases the lift coefficient. Placing a rotation rod immediately in front of or behind the cylinder (position angle =  $0^\circ$  or  $180^\circ$ ) causes a reduction in the lift coefficient for all rotation rates.

**Keywords:** flow control; rotating cylinder; control rod; circular cylinder; vortex shedding



**Citation:** Zhao, M.; Taheri, E. Control of Flow Past a Circular Cylinder Using a Rotating Control Rod. *J. Mar. Sci. Eng.* **2022**, *10*, 608. <https://doi.org/10.3390/jmse10050608>

Academic Editor: Giovanni Malara

Received: 8 April 2022

Accepted: 27 April 2022

Published: 29 April 2022

**Publisher's Note:** MDPI stays neutral with regard to jurisdictional claims in published maps and institutional affiliations.



**Copyright:** © 2022 by the authors. Licensee MDPI, Basel, Switzerland. This article is an open access article distributed under the terms and conditions of the Creative Commons Attribution (CC BY) license (<https://creativecommons.org/licenses/by/4.0/>).

## 1. Introduction

Suppression of vortex shedding in the wake of circular cylinders is of engineering importance because vortex-induced vibration (VIV) is a hazard for many engineering structures such as chimneys, offshore pipelines, power cables, heat exchanger tubes, etc. Many flow control methods for suppressing vortex shedding have been proposed, and they can be classified into two categories: active control and passive control. In active control, external energy is used to modify the boundary layers on the cylinder surface. Examples of active control include suction-based control [1], jet control [2,3], and controlled cylinder rotation [4]. Passive control involves controlling the flow by attaching small objects to the cylinder [5–7] or by modifying the geometry of the cylinder [8–10].

Proper placing of single or multiple control rods near a cylinder is believed to enable effective suppression of vortex shedding [11–13]. One flow control target is drag reduction. Firat et al. [7] conducted numerical simulations of flow past a square prism with an upstream control rod at  $d/D = 4$  and  $Re = 200$ , where  $D$  is the side length of a square prism (also called a square cylinder) or the diameter of a cylinder,  $d$  is the diameter of the control rod, and the Reynolds number is defined based on  $D$ . It was found that positioning a control rod at  $2D$  or  $3D$  upstream of the square prism can reduce the drag by 74% and the lift by up to 60%. Igarashi [14] conducted an experimental study of flow control by placing a control rod upstream of a square prism with various rod diameters and rod-to-prism spacings and derived an empirical formula to estimate the critical gap below which the vortex shedding from the control rod disappears. Yen and Wu [15] conducted an experimental study of a control rod upstream of a square cylinder and classified the vortex streets into single, attached, and bi-vortex streets by varying the Reynolds number and spacing ratio.

Placing a control rod in the wake of a cylinder can reduce the lift by interfering with the vortex dynamics. Gim, Kim et al. [16] conducted experiments on flow control in the

wake of a circular cylinder by placing a control rod at the rearward stagnation point, using the particle image velocimetry (PIV) technique for various rod diameters, and found that  $d/D = 0.3$  has an excellent effect on reducing turbulence intensity. Chauhan, Dutta et al. [17] conducted an experimental study of flow control using two small control rods in the shear layers behind a square cylinder, with  $d/D = 0.2$  and  $Re = 485$ , and achieved a maximum 22% drag reduction. Lu, Liu et al. [18] and Silva-Ortega and Assi [19] conducted numerical and experimental investigations of flow control using multiple control rods surrounding a circular cylinder. Silva-Ortega and Assi [19] found that the configuration of four control rods with a gap ratio of  $G/D = 0.05$  ( $G$  is the gap between the control rod and the main cylinder) and a diameter ratio of  $d/D = 0.06$  produced the lowest drag, compared to all other configurations. Lu, Liu et al. [18] classified the interference between the cylinder and rods into four flow regimes with varying suppression effectiveness and flow characteristics. Silva-Ortega and Assi [20] investigated the suppression of VIV using multiple rotating control rods.

Using rotating control rods was found to have great potential to further improve the effectiveness of flow control. Mittal [21] conducted two-dimensional numerical simulations of flow control using two small rotating rods on either side of the cylinder, with  $Re = 100$  and  $10^4$ , and found a significant reduction in the overall drag and lift forces. However, the power required to rotate the cylinder at  $Re = 100$  was much higher than that at  $Re = 10^4$ . Using numerical simulations of flow control using twin control rods symmetrically placed behind a circular cylinder at  $d/D = 0.2$  and  $Re = 150$ , Goodarzi and Dehkordi [22] and Goodarzi and Dehkordi [23] found the most effective positions for the rotating controllers for perfect suppression of vortex shedding. They reported that the most effective positions may vary for different engineering applications, and the presence of the rotating controllers usually resulted in the separation bubbles remaining attached to the system of cylinders. Schulmeister, Dahl et al. [12] conducted a similar study of flow control using two control rods behind the cylinder but with a smaller rod-to-cylinder distance. They found a recirculation region around the control rod. The streamline reattached to the main cylinder with greater pressure than at separation, resulting in increased base pressure and reduced pressure drag. Placing two control rods in the wake of a cylinder was also found to be effective for the suppression of VIV [24,25]. Oscillatory rotation of the circular cylinder itself at the proper frequency and velocity also has the potential to weaken vortex shedding and reduce lift [4,26].

The majority of the above-mentioned studies of flow control methods using control rods focus on wake control, with control rods placed in the wake of the cylinder to control the formation of wake vortices. It is expected that the mechanisms of flow control will be different when the rod is placed in different locations around the cylinder. In this study, the mechanisms of flow control using a small control rod at various angular positions along the cylinder surface were investigated by conducting numerical simulations. Specifically, the control effect of the rod on the fluid force was examined through its interference with formation of the shear layer when the rod is upstream of the cylinder and with the formation of the vortices when it is downstream of the cylinder. Extensive simulations with a variety of position angles of the control rod relative to the cylinder were conducted, and the reduction or increase in the coefficients of fluid force on the cylinder were quantified.

Figure 1a shows the use of a small rod (referred to as the rod hereafter) to control the flow around a cylinder with a diameter  $D$ . The rod has a diameter  $d$ , and its position relative to the cylinder is determined by a gap  $G$  and a position angle  $\beta$ . The angular rotational velocity is denoted by  $\sigma$ , which is positive in the anticlockwise direction. The nondimensional rotational speed is defined as  $\alpha = \sigma d / (2U)$ , where  $U$  is the free-stream velocity. This is referred to as the rotation rate hereafter. A Cartesian coordinate system  $Oxy$  is defined, with its origin located at the center of the cylinder and with the  $x$ -direction following the flow direction, as shown in Figure 1.

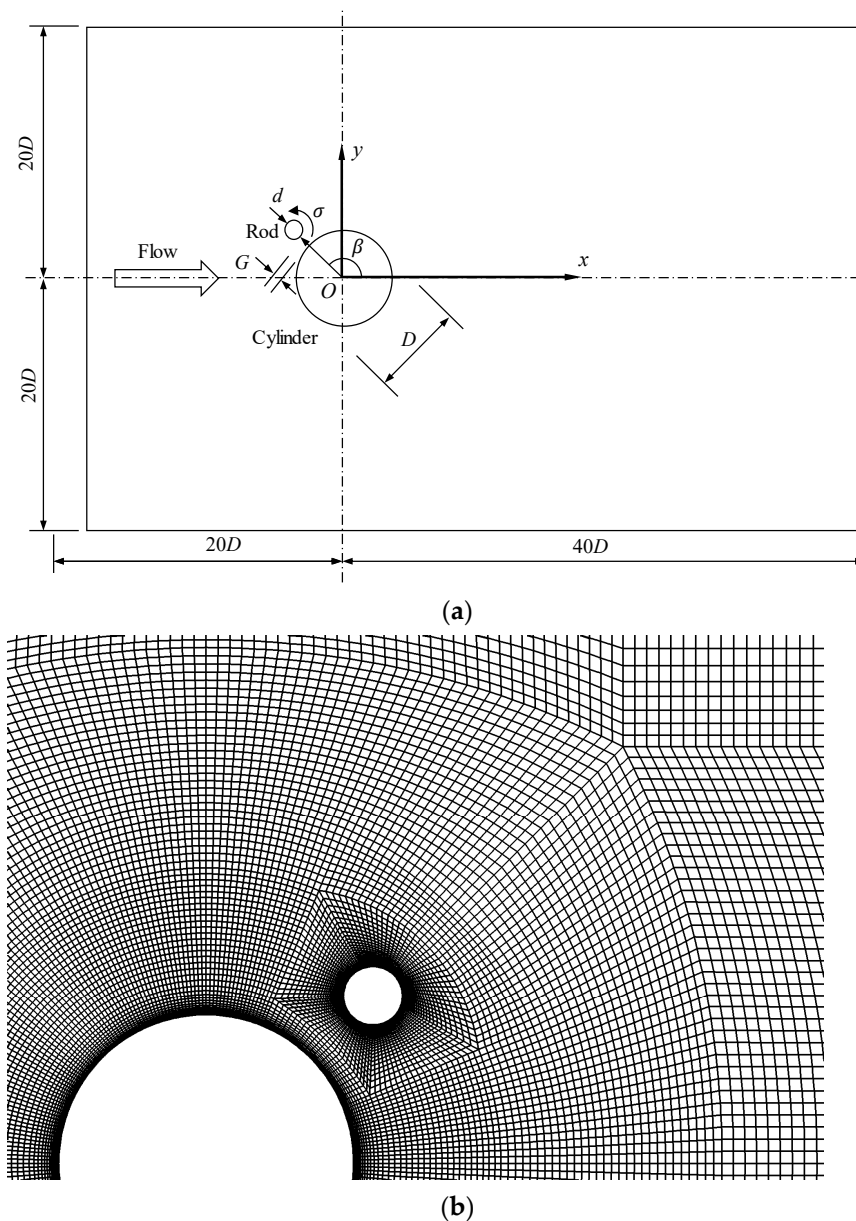


**Figure 1.** (a) Sketch of flow past a cylinder with a rotating control rod; (b) computational mesh near the cylinder and rod for  $\beta = 45^\circ$ .

In all the numerical simulations, the Reynolds number, the diameter ratio, and the gap ratio were  $Re = 200$ ,  $d/D = 0.2$ , and  $G/D = 0.2$ , respectively. The Reynolds number is defined as  $Re = UD/\nu$ , where  $U$  and  $\nu$  are the fluid velocity and kinematic viscosity of the fluid, respectively. Vortex shedding occurred as  $Re$  exceeded 40, and was two-dimensional until the Reynolds number exceeded a critical value. The critical  $Re$  for transitioning from two-dimensional to three-dimensional flow varied between 140 to 194, depending on the disturbance in the flow in the experiments [27]. The three-dimensional numerical study by Zhao, Thapa et al. [28] indicated that the flow was in the two-dimensional flow regime up to  $Re = 200$ , and the lift coefficient of the cylinder increased with an increase in  $Re$ . In this paper, a Reynolds number of 200 was studied, because this Reynolds number is the highest Reynolds number with the largest lift coefficient in the two-dimensional regime. The focus of the study was to investigate the effects of the position angle  $\beta$  and the rotation rate on the wake flow and lift coefficient. To achieve this, simulations were conducted for  $\beta = 0^\circ, 45^\circ, 90^\circ, 135^\circ$ , and  $180^\circ$ , with rotation rates ( $\alpha$ ) ranging from  $-7$  to  $7$  and an interval of  $0.2$ .

## 2. Numerical Method

The fluid was assumed to be an incompressible Newtonian fluid. The velocity, the time, and the pressure were nondimensionalized as  $(u, v) = (\tilde{u}, \tilde{v})/U_m$ ,  $t = \tilde{t}U/D$ , and pressure  $p = \tilde{p}/(\rho U^2)$ , where  $u$  and  $v$  are the fluid velocity components in the  $x$ - and  $y$ -directions, respectively,  $U$  is the fluid velocity, and  $p$  is the pressure. In this paper, a wave dash ‘~’ on top of a variable represents a dimensional value. The nondimensional and two-dimensional Navier–Stokes (NS) equations are:

$$\frac{\partial u}{\partial x} + \frac{\partial v}{\partial y} = 0 \tag{1}$$

$$\frac{\partial u}{\partial t} + u \frac{\partial u}{\partial x} + v \frac{\partial u}{\partial y} = -\frac{\partial p}{\partial x} + \frac{1}{Re} \left( \frac{\partial^2 u}{\partial x^2} + \frac{\partial^2 u}{\partial y^2} \right) \tag{2}$$

$$\frac{\partial v}{\partial t} + u \frac{\partial v}{\partial x} + v \frac{\partial v}{\partial y} = -\frac{\partial p}{\partial y} + \frac{1}{Re} \left( \frac{\partial^2 v}{\partial x^2} + \frac{\partial^2 v}{\partial y^2} \right) \tag{3}$$

The NS equations were solved by the finite element method (FEM) and the corresponding in-house software developed by Zhao, Cheng et al. [29]. The detailed FEM formulae can be found in Zhao, Cheng et al. [29] and will not be presented here. A rectangular computational domain with a length of  $60D$  and a width of  $40D$  was used, and the cylinder was located  $20D$  downstream of the left boundary. Behr, Hastreiter et al. [30] reported that the blockage ratio, i.e., the ratio of the cylinder diameter to the width of the computational domain, must be less than 0.0625, to ensure there is no blockage effect from the two lateral boundaries. The blockage effect in this paper was considered to be negligible, because the largest blockage ratio at  $\beta = 90^\circ$  was 0.03, which is less than half of the value recommended by Behr, Hastreiter et al. [30].

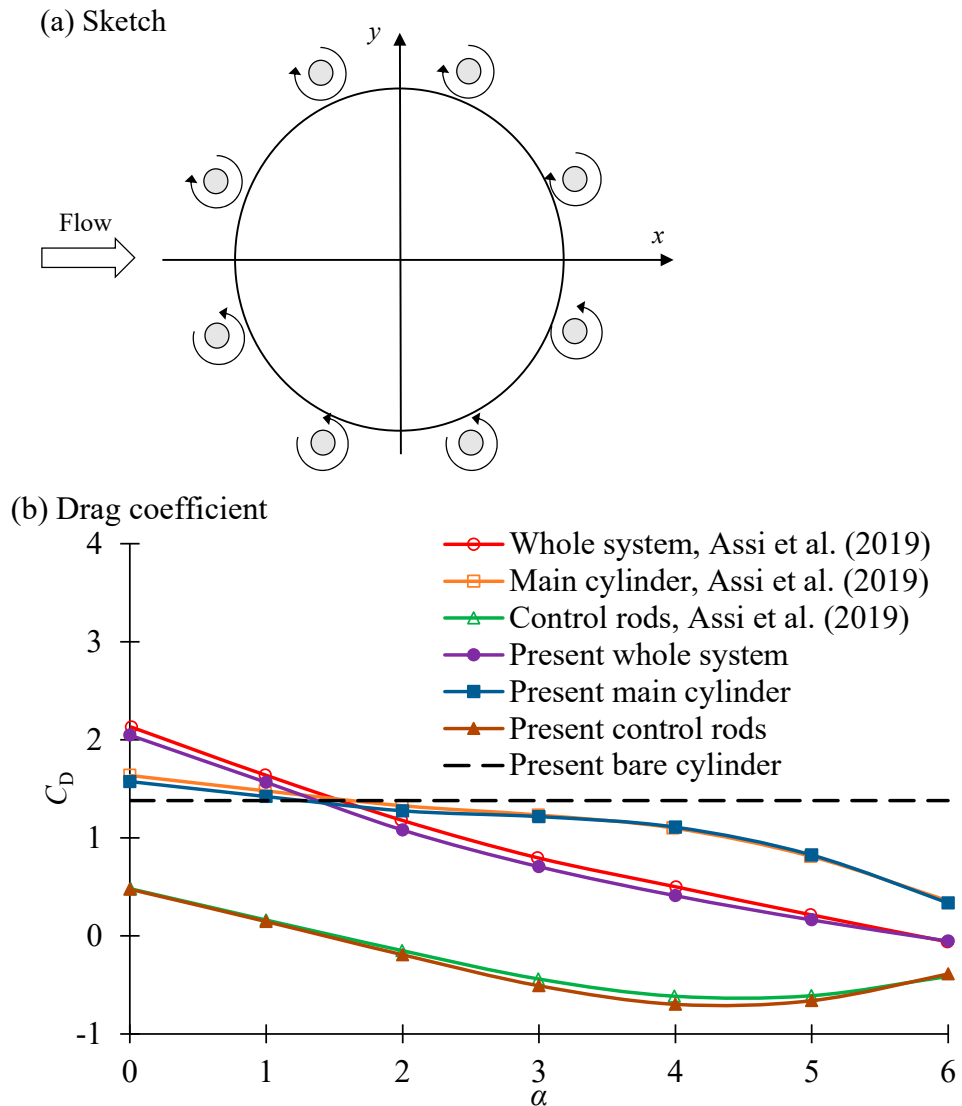
The boundary conditions for solving the equations were specified as follows. On the inlet boundary, the velocity was given and the pressure gradient in the  $x$ -direction was zero. On the outlet (right) boundary, the pressure was zero and the gradient of the velocity in the  $x$ -direction was zero [31,32]. On the top and bottom boundaries, free-slip boundaries were used, i.e., the velocity in the  $y$ -direction was zero and the gradients in the  $y$ -direction of the pressure and the  $x$ -velocity were zero. The fluid velocity was zero on the cylinder surface and the same as the rod’s rotation velocity on the rod’s surface. The gradient of the pressure normal to the wall surface was zero.

Figure 1b shows the computational mesh near the cylinder and rod for  $\beta = 45^\circ$ . The whole computational domain was divided into 47,468 structured quadrilateral 4-node linear finite elements. The surfaces of the cylinder and rod were divided into 288 and 136 finite elements, respectively, and the minimum nondimensional element size in the radial direction on the wall surfaces was 0.002.

## 3. Numerical Validation and Mesh Dependency Study

The nondimensional computational time was  $\Delta t = 0.00025$ . Zhao [33] and Zhao, Cheng et al. [34] performed a detailed validation of the numerical model for flow past one and two cylinders at  $Re = 200$  and flow past a rotating cylinder at  $Re = 200$ , respectively. Data for one cylinder with one control rod are not available for validation. However, we validated our model using the numerical results for the flow past eight control rods presented by Assi, Orselli et al. [35]. The additional numerical simulations of the flow past a circular cylinder with eight control rods shown in Figure 2a were conducted for the purpose of validation. The diameter ratio, the Reynolds number, and the gap ratio were  $d/D = 0.05$ ,  $Re = 100$ , and  $G/D = 0.05$ , respectively. The eight control rods rotated at the same rate, but the top four rods rotated in the clockwise direction and the bottom four rods rotated in the anticlockwise direction. The coefficients of drag and lift on the cylinder were defined as  $C_{DC} = F_{DC}/(\rho DU^2/2)$  and  $C_{LC} = F_{LC}/(\rho DU^2/2)$ , where  $F_{DC}$  and  $F_{LC}$  are the drag and lift forces of the cylinder, respectively. The coefficients of drag and lift on the rod were

defined as  $C_{DR} = F_{DR}/(\rho DU^2/2)$  and  $C_{LR} = F_{LR}/(\rho DU^2/2)$ , where  $F_{DR}$  and  $F_{LR}$  are the drag and lift forces on the rod, respectively. An overbar and a prime on a force coefficient denote the mean value and the standard deviation (SD) of the force coefficient, respectively. For example,  $\bar{C}_{DC}$  and  $\bar{C}_{LC}$  denote the mean drag and lift coefficients on the cylinders, and  $C'_{DC}$  and  $C'_{LC}$  denote the standard deviations of the drag and lift coefficients on the cylinder, respectively.



**Figure 2.** Comparison between present numerical results and the numerical results in Ref. [35] for flow past one cylinder with eight control rods at  $d/D = 0.05$ ,  $Re = 100$ , and  $G/D = 0.05$

Figure 2 shows the mean drag coefficient as a function of the rotation rate in comparison with the numerical results in [35]. The drag coefficient on the control rods is the sum of the drag coefficients of all the eight rods in the figure. The mean drag coefficient of the whole system is greater than that of a bare cylinder at  $\alpha = 0$  and 1. With an increase in  $\alpha$ , the mean drag coefficient continuously decreases, becoming slightly smaller than zero at  $\alpha = 6$ . The variation trend presented in the numerical results agrees with that in [35], with only a very small difference. We further reduced the mesh density but did not obtain results that were closer to those of [35]. The relative error between the two sets of results was defined as  $diff = (C_{D,present} - C_{D,Assi})/C_{D,bar\ cylinder}$ . In the whole range of  $0 \leq \alpha \leq 6$ , the maximum values of  $diff$  of the drag coefficients of the whole system, the main cylinder, and the rods were 0.073, 0.045, and 0.060, respectively.

To ensure the density of the mesh was sufficiently small to obtain a converged solution, a mesh dependency study was conducted by performing simulations for  $\beta = 90^\circ$  and the largest rotation rate of  $\alpha = 7$ , using three additional meshes, and the results for the force coefficients are listed in Table 1. The density of each mesh is characterized by the total finite element number  $N_{element}$ , the element number along the cylinder  $N_{e,cylinder}$ , the element number along the rod  $N_{e,rod}$ , and the mesh size in the radial direction on the cylinder and rod  $\Delta_{r1}$ . The normal mesh is the one used for all the simulations in this study.

**Table 1.** Statistical values of the drag and lift coefficients in the mesh dependency study for  $\beta = 90^\circ$  and  $\alpha = 7$ .

Cylinder	Mesh	$N_{element}$	$N_{e,cylinder}$	$N_{e,rod}$	$\Delta_{r1}$	$\bar{C}_{DC}$	$\bar{C}_{LC}$	$C'_{DC}$	$C'_{LC}$
	dense	81,468	320	136	0.001	2.402	-0.188	0.303	1.277
	normal	47,468	288	100	0.002	2.421	-0.190	0.302	1.283
	coarse	35,678	256	82	0.003	2.340	-0.186	0.290	1.240
	coarser	30,185	224	80	0.004	2.300	-0.173	0.287	1.220
Rod	Mesh	$N_{element}$	$N_{e,cylinder}$	$N_{e,rod}$	$\Delta_{r1}$	$\bar{C}_{DR}$	$\bar{C}_{LR}$	$C'_{DR}$	$C'_{LR}$
	dense	81,468	320	136	0.001	2.332	-0.324	0.836	0.376
	normal	47,468	288	100	0.002	2.367	-0.329	0.840	0.381
	coarse	35,678	256	82	0.003	2.233	-0.315	0.798	0.368
	coarser	30,185	224	80	0.004	2.249	-0.299	0.803	0.370

It can be seen from Table 1 that the force coefficients from the dense and the normal meshes were very close to one another. The differences in  $\bar{C}_D, \bar{C}_L$ , and  $C'_L$  for the dense and normal meshes were 0.78%, 1.05%, 0.33%, and 0.47, respectively. The results from the coarse and dense meshes also showed little difference from one another. To prove that  $\Delta t = 0.00025$  was sufficiently small for obtaining accurate results, the effects of the nondimensional computational time step  $\Delta t$  on the results were also studied, by conducting simulations at  $\beta = 90^\circ$  and  $\alpha = 7$  using normal mesh under three different computational time steps of  $\Delta t = 0.00025, 0.0005$ , and  $0.001$ . As seen in Table 2, the differences in  $\bar{C}_D, \bar{C}_L, C'_D$ , and  $C'_L$  for  $\Delta t = 0.00025$  and  $0.0005$  were 0.41%, 0.53%, 0.33%, and 0.07, respectively.

**Table 2.** Statistical values of the drag and lift coefficients in the time-step dependency study for  $\beta = 90^\circ$  and  $\alpha = 7$ .

Cylinder	$\Delta t$	$\bar{C}_D$	$\bar{C}_L$	$C'_D$	$C'_L$
	0.00025	2.421	-0.190	0.302	1.283
	0.0005	2.420	-0.189	0.301	1.284
	0.0010	2.411	-0.189	0.303	1.271
Rod	$\Delta t$	$\bar{C}_{DR}$	$\bar{C}_{LR}$	$C'_{DR}$	$C'_{LR}$
	0.00025	2.367	-0.329	0.840	0.381
	0.0005	2.360	-0.320	0.841	0.388
	0.0010	2.360	-0.300	0.841	0.388

#### 4. Results

Figure 3 shows the variation in the standard deviations (SD) of the lift and drag coefficients with rotation rate. The total drag and total lift coefficients were defined as  $C_D = (F_{DC} + F_{DR}) / (\rho D U^2 / 2)$  and  $C_L = (F_{LC} + F_{LR}) / (\rho D U^2 / 2)$ , respectively. The mean and SD of the force coefficients were obtained using the data within 10 vortex shedding periods. The variation in the SD of the lift coefficient of the cylinder was very similar to

that of the total lift coefficient for all the position angles of the rod, except that the SD of the total lift coefficient was slightly greater than the SD of the lift coefficient of the cylinder. The best reduction in the SD of the lift coefficient occurred for  $\alpha \leq -4$ , for all the position angles of the rod.

To give a clear view of the very small SD of the drag coefficients for all the negative rotation rates, a view with a small vertical axis scale is presented in Figure 3d. It can be seen that  $C'_D$ , in the range of  $\alpha \leq -4$ , was increased by around 50% to 100% for  $\beta = 0^\circ, 135^\circ$ , and  $180^\circ$ . However, the increase in the SD of the drag coefficient was minimal, since it was insignificantly smaller than the SD of the lift coefficient. The SD of the drag on the cylinder ( $C'_{DC}$ ) was increased significantly for  $-4 \leq \alpha \leq -3$ , but the SD of the total drag ( $C'_D$ ) was not, because the drag coefficients on the cylinder and rod were out of phase with each other.

The SD of both the drag and lift coefficients were increased dramatically when the rotation rate was positive with a high magnitude. Positive rotation rates have not been considered in many studies of flow control using rotating rods [12,22]. If vortex-induced vibration is utilized for energy harvesting, using a positive rotation of the rod would increase the energy significantly [36].

When a uniform flow approaches the cylinder, shear layers generated on the cylinder surface form vortex shedding, which causes oscillation of the fluid force on the cylinder. To explain the effects of the control rod on the drag and lift coefficient, the flow was visualized using the contours of vorticities and streamlines. The nondimensional vorticity is defined as  $\omega = \partial v / \partial x - \partial u / \partial y$ . In the following discussion, shear layers whose vorticities are positive and negative are referred to as positive and negative shear layers, respectively. At  $\beta = 180^\circ$ , the SD of the drag and lift coefficients reduced suddenly as the rotation rate  $\alpha$  increased from 3.2 to 3.4, as shown in Figure 3. The instantaneous flows at  $\alpha = 2.4$  and 3.6 shown in Figure 4 explain the sudden reduction. In Figure 3a,b, where  $\alpha = 2.4$ , the rotating control rod did not have a significant effect on the shear layer formed on the cylinder surface, and the vortex shedding from the cylinder resembled that of a cylinder without control rods. The SD of the lift coefficient of the cylinder in Figure 3a was close to that of a single cylinder at  $\alpha = 2.4$ . In Figure 3c,d, where the total lift coefficient of both cylinders reached its maximum and minimum values, respectively, the rotation rate of the control rod was so large that it caused the negative shear layer to separate from the top side surface of the cylinder, forming a vortex and finally reattaching to the cylinder surface again behind the vortex, as indicated in Figure 3c,d. The separation and reattachment of the shear layer on the top surface of the cylinder weakened the vortex shedding, and the lift coefficient was weakened significantly.

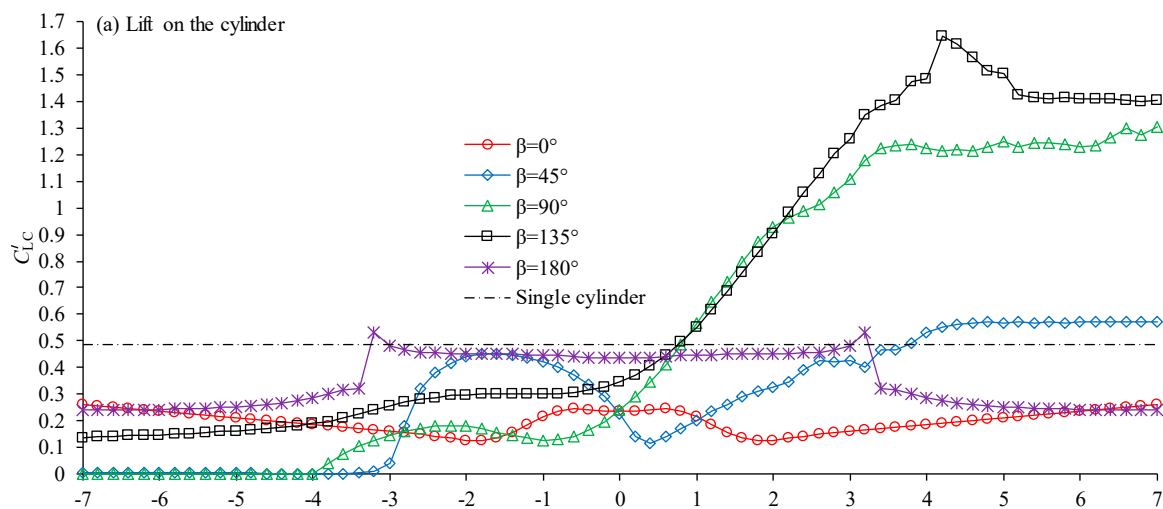


Figure 3. Cont.

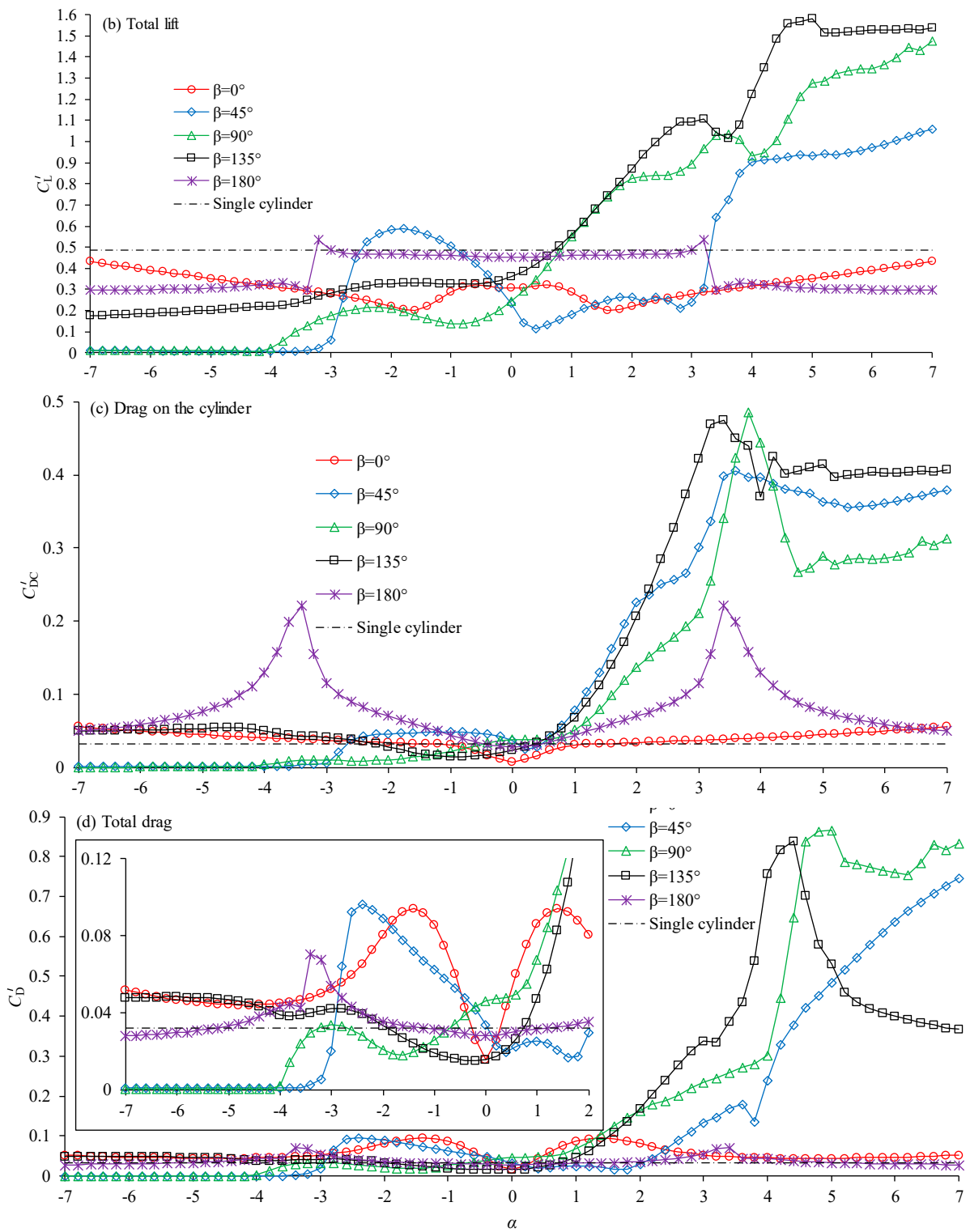
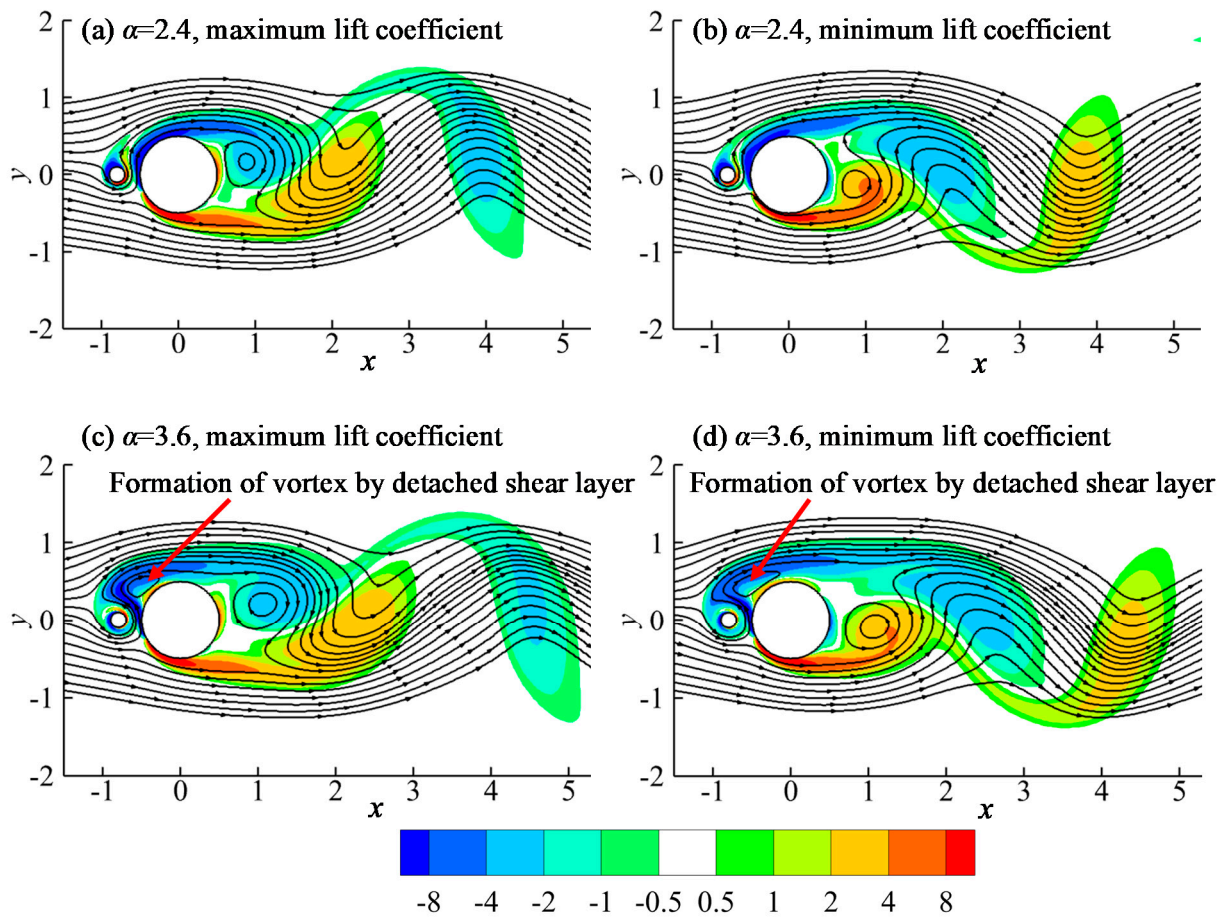


Figure 3. Variation of the drag and lift coefficients with  $\alpha$ .



**Figure 4.** Streamlines and the contours of the nondimensional vorticity of instantaneous flows when the lift coefficient reaches its maximum and minimum values for  $\beta = 180^\circ$ .

To further understand the effects of the rotating rod on the flow and the force coefficients, the streamlines and the contours of the vorticity based on the mean flow are discussed, and the correlation between the flow and force coefficients analyzed. The mean flow is the averaged flow over one vortex shedding period. Because the vortex shedding flow is periodic for all the simulated cases, one vortex shedding period of flow data is sufficient to obtain the time-averaged mean flow. The flow structures for the three position angles  $\beta = 45^\circ, 90^\circ$ , and  $135^\circ$  are discussed together because they share similar flow characteristics and vortex dynamics. Figures 5–7 show the streamlines and nondimensional vorticity contours of the mean flow for  $\beta = 45^\circ, 90^\circ$ , and  $135^\circ$ , respectively. The nondimensional vorticity is defined as  $\omega^* = (\partial v / \partial x - \partial u / \partial y) / (U / D)$ , where  $u$  and  $v$  are the velocity components in the  $x$ - and  $y$ -directions, respectively.

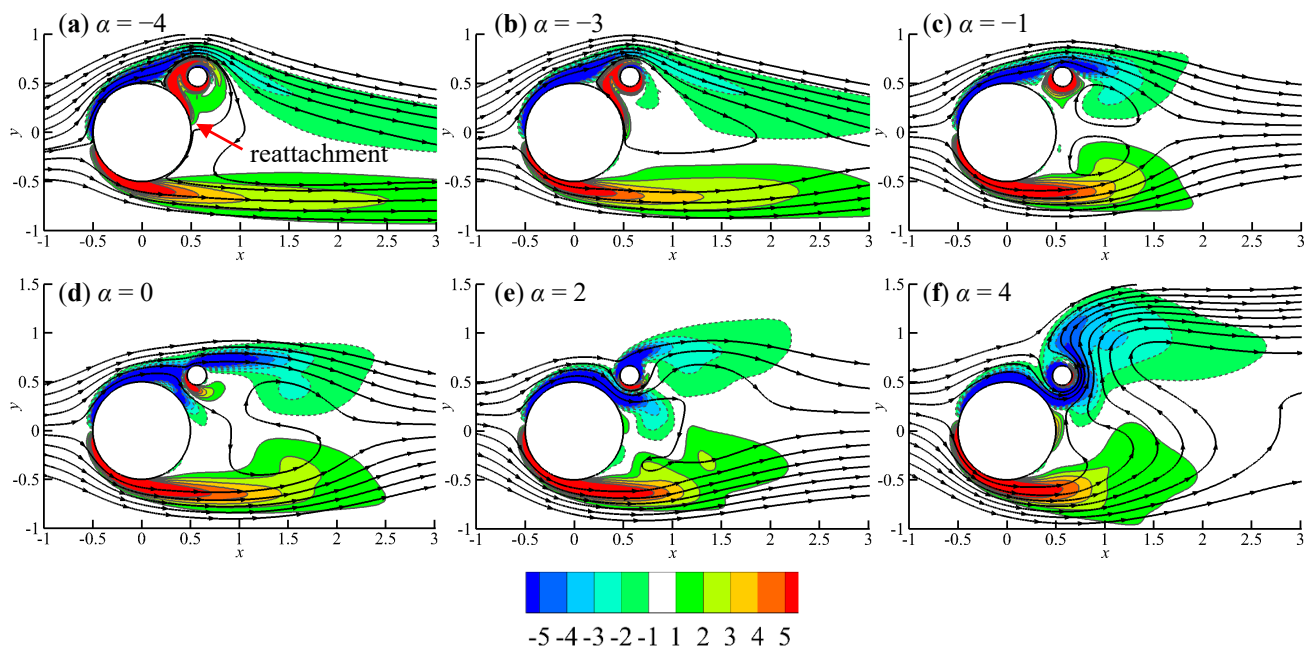


Figure 5. Streamlines and the contours of the nondimensional vorticity of the mean flow for  $\beta = 45^\circ$ .

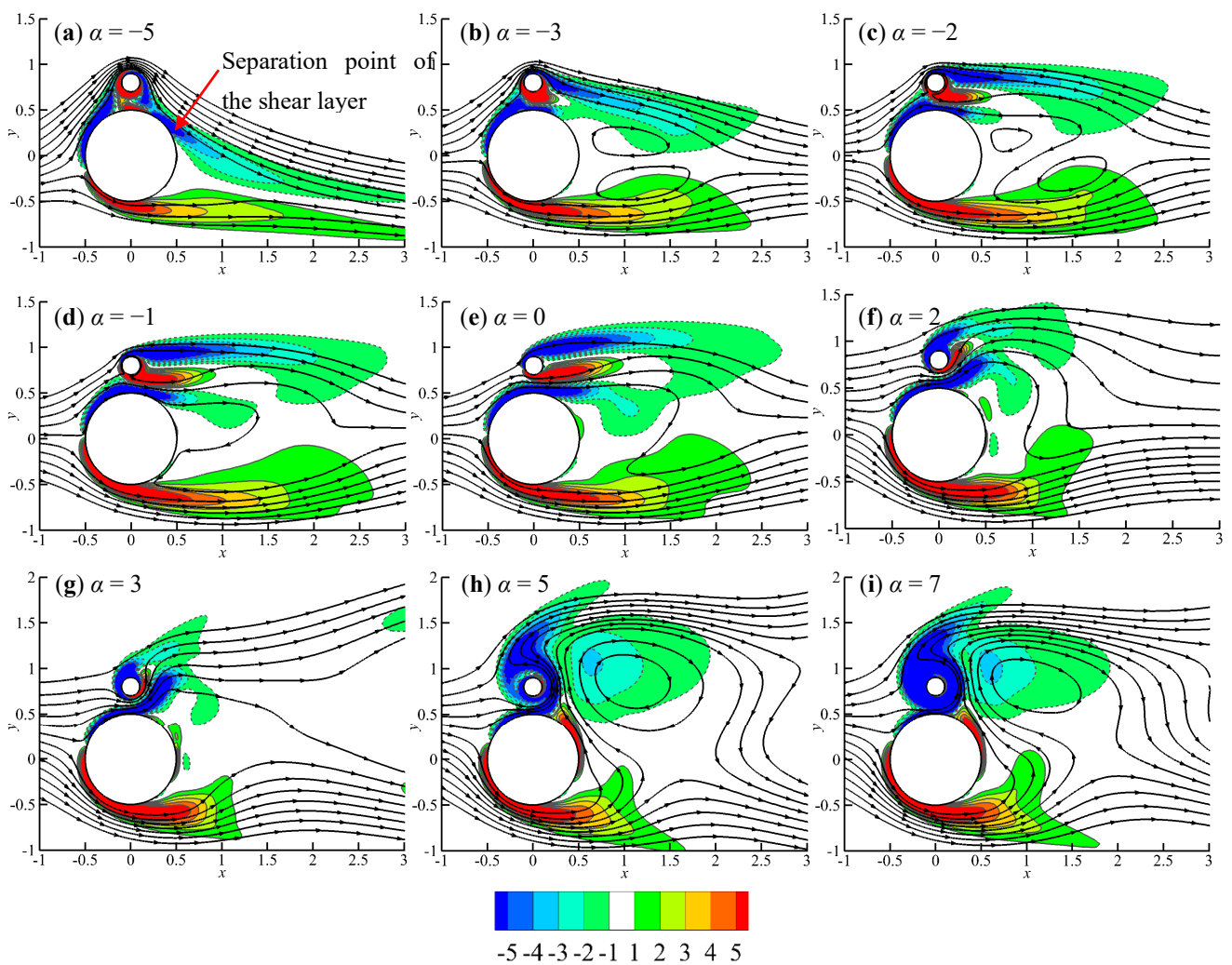
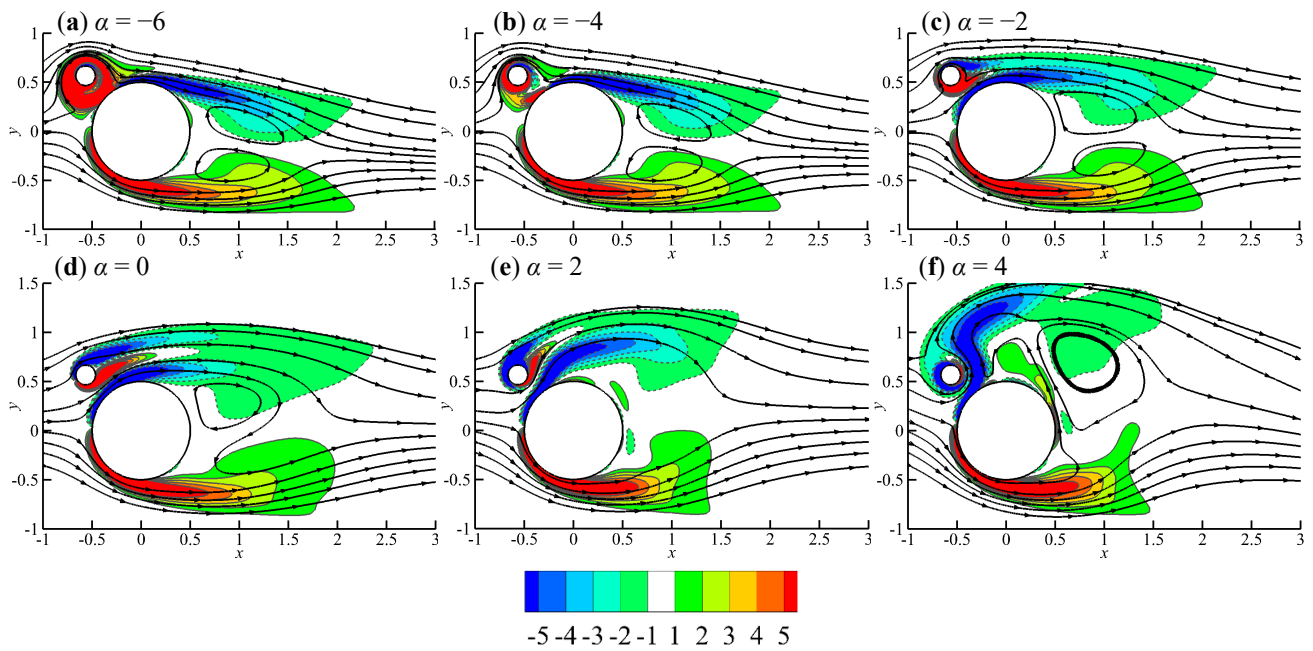


Figure 6. Streamlines and the contours of the nondimensional vorticity of the mean flow for  $\beta = 90^\circ$ .



**Figure 7.** Streamlines and the contours of the nondimensional vorticity of the mean flow for  $\beta = 135^\circ$ .

The wake vortex shedding was mainly caused by the separated negative shear layers from the top of the cylinder and rod, and the positive shear layer from the bottom of the cylinder. For  $\beta = 45^\circ$ , the negative shear layer from the top of the rod could be one that had separated from the cylinder previously and had reattached to the rod (Figure 5). The rotation of the rod affected the flow by modifying the negative shear layers from the tops of the rod and cylinder. Positive vorticity around the rod caused by negative rotation weakened the negative shears and vice versa. The rotation of the rod at an excessively high negative rotation rate caused disappearance of the separated negative shear layer, as shown in Figure 7a. The rotation of the rod at a very large positive rotation rate caused the disappearance of the positive shear layer, and as a result, the negative shear layer from the rod became stronger, as shown in Figure 7f. By observing the mean flow structures and the lift coefficient in Figures 5 and 6, the rotation of the rod can be seen to affect the flow via the following three mechanisms:

- Strong negative rotation of the rod weakens the negative free shear layers;
- Flow through gap interferes with vortex shedding;
- Strong positive rotation of the rod enhances the negative free shear layers.

In one case, two of the above three mechanisms may co-exist and affect the flow. In the following, these three mechanisms will be discussed in detail.

#### 4.1. Reduction of the Negative Free Shear Layers by Strong Negative Rotation of the Rod

Negative rotation of the rod generated positive vorticity, which in turn weakened the negative shear layers from both the cylinder and the rod. In Figures 6a and 7a,b, the magnitude of the negative rotation rate was so high that the negative shear layer from the rod was totally cancelled out. As the result, the shear layer regenerated behind the rod did not have sufficient strength to form vortices, and the vortex shedding was fully suppressed. The full suppression of vortex shedding is evidenced by the zero standard deviation of the lift coefficient in Figure 3. In the study of flow control using two rotating rods, with  $d/D = 0.05$  on either side of the cylinder at  $Re = 100$ , Mittal [21] also found a steady flow condition at  $\alpha = 5$ .

When  $\beta = 45^\circ$ , as shown in Figure 5a,b, the negative shear layer, which was developed over a longer distance on the cylinder surface before it reached the rod, was not fully suppressed at  $\alpha = -6$  and  $-4$ , though it was significantly weakened. The weakened negative shear layer from the top of the rod reduced the strength of the vortices and the lift

coefficient. For  $\beta = 135^\circ$ , the upstream location of the rod allowed a new negative shear layer to be regenerated from the upstream surface of the cylinder, as shown in Figure 7a,b, and allowed it to exist over a long distance along the cylinder. As a result, full suppression of the vortex shedding was not observed.

As the magnitude of the negative rotation rate was reduced, the negative shear layer from the top of the rod became stronger, and so did the negative vortices formed. As a result, the lift coefficient increased, as shown in Figure 3a. However, the lift coefficient started to decrease at  $\alpha \geq -2$  for  $\beta = 90^\circ$  and  $\alpha \geq -2.2$  for  $\beta = 45^\circ$ . This was due to the interference of the flow through the gap.

#### 4.2. Interference of Flow through Gap with Vortex Shedding

When the rod rotated in the negative direction with a sufficiently large rotation rate, no fluid flowed through the gap. Fluid flowed through the gap when the magnitude of the negative rotation rate was reduced to a certain level, i.e.,  $\alpha > -1$ ,  $-4$  and  $-3.4$  for  $\beta = 45^\circ$ ,  $90^\circ$ , and  $135^\circ$ , respectively. Fluid flow through the gap generated positive and negative shear layers from the rod and the cylinder, respectively. The gap flow increased as the magnitude of negative  $\alpha$  decreased. The strong positive shear layer from the bottom of the rod interfered with and weakened the vortex shedding process, as shown in Figures 5d, 6d and 7d. The minimum values of the lift coefficient at  $\alpha = 0.4$  and  $\alpha = -0.8$  for  $\beta = 45^\circ$  and  $90^\circ$ , respectively, were caused by the interference of the flow through the gap.

For  $\beta = 135^\circ$ , the positive shear layer from the bottom of the rod did not affect the vortex shedding process as much as for  $\beta = 90^\circ$ , because it was weakened significantly before it reached the topmost point of the cylinder. Nevertheless, its interference resulted in the lift coefficient increasing with  $\alpha$  much more slowly in the range of  $-2 \leq \alpha \leq -1$ . For  $\beta = 135^\circ$ , the interference of the gap flow with the vortex shedding was very weak, because the position of the gap allowed only very small volumes of fluid to flow into the gap. As a result, the minimum value of the lift coefficient caused by the interference of the flow through the gap was not observed.

#### 4.3. Enhancement of the Negative Free Shear Layer by Strong Positive Rotation of the Rod

When the rotation rate of the rod was positive, the lift coefficient increased with an increase in the rotation speed, because the positive rotation enhanced the negative shear layer from the top of the cylinder, which was responsible for the generation of negative wake vortices, and at the same time weakened the positive shear layer from the bottom of the rod. When the positive shear layer in the gap was sufficiently weak (Figures 5e, 6f and 7e), the two negative shear layers combined and formed a stronger negative shear layer. If the positive rotation rate of the rod was sufficiently large, strong negative vorticity around the rod fed into the negative shear layer on top of the cylinder, as shown in Figures 5f, 6i and 7f, resulting in a significant increase in the wake vortices and the lift coefficient.

Placing the rod in the wake of the cylinder ( $\beta = 0^\circ$ ) reduced the lift coefficient by half or more, regardless of the rotation direction or rotation rate, because the rod mitigated the interaction between the negative and positive vortices in the wake [16].

For  $\beta = 180^\circ$ , the reduction in the lift coefficient caused by the rotation of the rod was found to be significant for  $|\alpha|$  greater than 3.4 and very small for  $|\alpha|$  smaller than 3.2. The lift coefficient was reduced significantly when  $|\alpha| \geq 3.4$ , because the positive shear layer on the bottom side of the cylinder separated and reattached to the cylinder surface, as indicated in Figure 8d–f. The separation of the shear layer for a certain distance before it reattached to the cylinder reduced its strength and consequently weakened the vortex shedding. For  $|\alpha| < 3.2$ , the rotation of the rod did not cause a large change in the lift coefficient, because it enhanced the positive shear layer and at the same time weakened the negative shear layer on the cylinder surface.

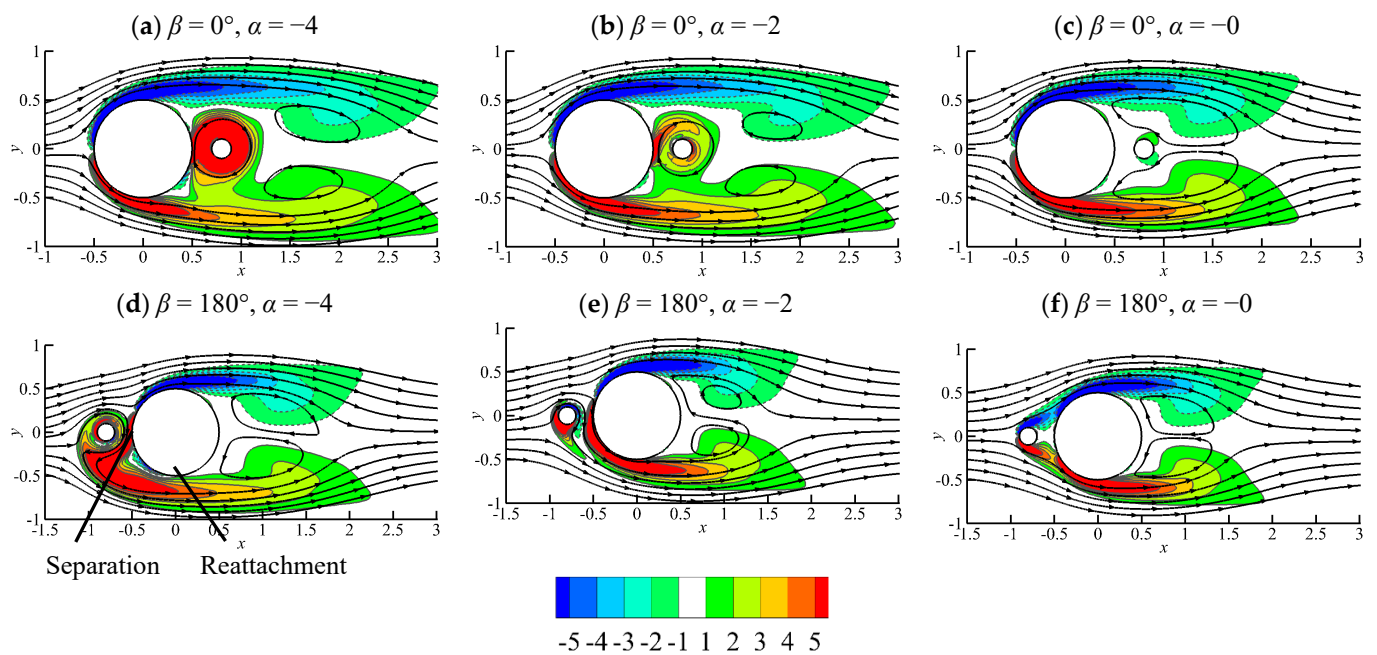


**Figure 8.** Streamlines and the contours of the nondimensional vorticity of the mean flow for  $\beta = 0^\circ$  and  $180^\circ$ .

Figure 9 shows the variation in the mean lift and drag coefficients with rotation rate. An overbar on  $C_D$  and  $C_L$  denotes the mean value. Both the mean lift coefficient of the cylinder and the total lift coefficient were significantly increased at large rotation rates, either in the negative or positive directions. The mean lift coefficient for the highest  $|\alpha|$  was greater than the mean drag coefficient for  $\beta = 45^\circ$ . A net lift coefficient could be avoided by placing two control rods either side of the cylinder. The mean total drag coefficient at large negative rotation rates was reduced compared with the case without a control rod.

Figure 10 shows the position angle of the stagnation point upstream of the cylinder ( $\theta_s$ ), which is referred to as the stagnation angle. The stagnation angle is  $180^\circ$  if the control rod does not exist. It can be seen that for  $\beta = 0^\circ, 45^\circ$ , and  $90^\circ$ , the stagnation point in front of the cylinder shifted downwards ( $\theta_s > 180^\circ$ ) if  $\alpha$  was negative and upwards ( $\theta_s < 180^\circ$ ) if  $\alpha$  was positive. The downward and upward shift of the stagnation point caused positive and negative net lift coefficients, respectively. The effect of the rotation direction on the stagnation point for  $\beta = 135^\circ$  and  $180^\circ$  was opposite to that for  $\beta = 0^\circ, 45^\circ$ , and  $90^\circ$ , i.e., a negative and positive  $\alpha$  caused an upward and downward shift of the stagnation point, respectively, on the front surface of the cylinder.

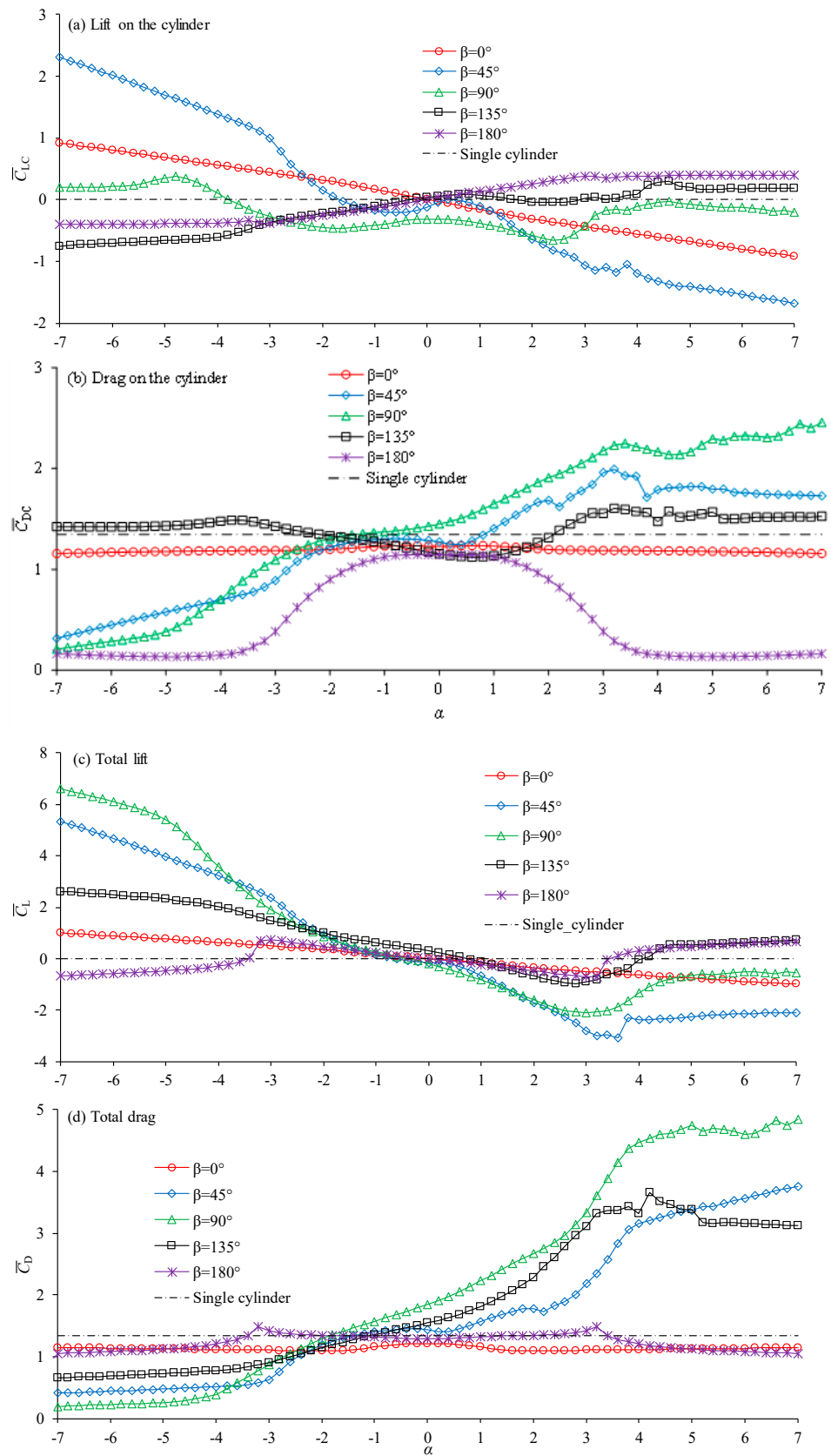


Figure 9. Variation in the mean lift and drag coefficients with rotation rate.

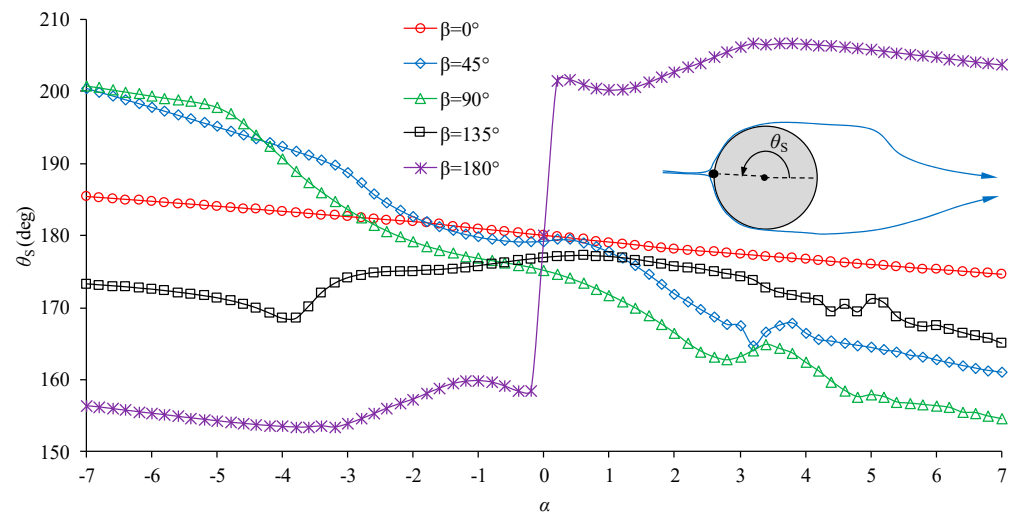


Figure 10. Variation in the angle of the stagnation point with rotation rate.

### 5. Conclusions

The effectiveness of flow control using a rotating control rod was investigated through two-dimensional numerical simulations for  $Re = 200$ ,  $d/D = 0.2$ ,  $G/D = 0.2$ , and  $\beta = 0^\circ, 45^\circ, 90^\circ, 135^\circ$ , and  $180^\circ$ . Simulations were conducted for a wide range of rotation rates between  $-7$  and  $7$ . The study was focused on the interference of the rod with the shear layers in cases where the rod was very close to the cylinder. The main conclusions can be summarized as follows.

When the rod was placed at the side ( $\beta = 90^\circ$ ), or nearly to the side of the cylinder ( $\beta = 45^\circ$  and  $135^\circ$ ), its rotation interfered with the shear layers in the following three ways, depending on the rotation rate: (1) strong negative rotation of the rod weakened the negative free layers, and as a result, the lift coefficient was reduced strongly; (2) the interference of the flow through the gap weakened the vortex shedding and reduced the lift coefficient; and (3) strong positive rotation of the rod enhanced the negative free shear layers and increased the lift coefficient.

The SD of the lift coefficient was significantly reduced for a rotation rate  $|\alpha| \leq -4$  for all the position angles. The vortex shedding could be fully suppressed for  $\beta = 90^\circ$  and  $45^\circ$  if the magnitude of the negative rotation rate was sufficiently large. A positive rotation rate caused a significant increase in the SD of the drag and lift coefficients if  $\beta = 45^\circ, 90^\circ$ , or  $135^\circ$ . Rotation of the rod with  $\beta = 0^\circ$  and  $180^\circ$  caused a reduction in the SD of the lift coefficient, regardless of rotation rate.

The rotation of the cylinder in either the negative or positive direction created a mean lift coefficient on the cylinder, which increased as the rotation rate increased. The mean total drag coefficient at a large negative rotation rate was reduced compared with the case without a control rod.

**Author Contributions:** Conceptualization, M.Z. and E.T.; methodology, M.Z.; software, M.Z.; validation, M.Z., and E.T.; investigation, M.Z., and E.T.; resources, M.Z.; writing—original draft preparation, M.Z., and E.T.; writing—review and editing, M.Z., and E.T.; supervision, M.Z. All authors have read and agreed to the published version of the manuscript.

**Funding:** This research received no external funding.

**Informed Consent Statement:** Not applicable.

**Data Availability Statement:** Data is contained within the article.

**Conflicts of Interest:** The authors declare no conflict of interest.

## Nomenclature

$C_D$	Drag coefficient
$C_L$	Lift coefficient
$C_{DC}$	Drag coefficient of the cylinder
$C_{DR}$	Drag coefficient of the control rod
$C_{LC}$	Lift coefficient of the cylinder
$C_{LR}$	Lift coefficient of the control rod
$D$	Diameter of the cylinder
$D$	Diameter of the control rod
$F_D$	Drag force
$F_L$	Lift force
$F_{DC}$	Drag force of the cylinder
$F_{DR}$	Drag force of the control rod
$F_{LC}$	Lift force of the cylinder
$F_{LR}$	Lift force of the control rod
$G$	Gap between the cylinder and the control rod
$P$	Pressure
$U$	Free-stream flow velocity
$Re$	Reynolds number
$SD$	Standard deviation
$U$	Velocity in the x-direction
$v$	Velocity in the y-direction
$x$	Coordinate in the streamwise direction
$y$	Coordinate in the crossflow direction
$\alpha$	Rotational rate
$\beta$	Position angle of the control rod
$\sigma$	Angular speed of the rotating rod
$\nu$	Kinematic viscosity of the fluid
$\omega$	Viscosity
$\Delta t$	Computational time step

## References

- Chen, W.-L.; Xin, D.-B.; Xu, F.; Li, H.; Ou, J.-P.; Hui, L. Suppression of vortex-induced vibration of a circular cylinder using suction-based flow control. *J. Fluids Struct.* **2013**, *42*, 25–39. [\[CrossRef\]](#)
- Feng, L.-H.; Wang, J.-J. The virtual aeroshaping enhancement by synthetic jets with variable suction and blowing cycles. *Phys. Fluids* **2014**, *26*, 014105. [\[CrossRef\]](#)
- Feng, L.-H.; Wang, J.-J. Modification of a circular cylinder wake with synthetic jet: Vortex shedding modes and mechanism. *Eur. J. Mech.-B/Fluids* **2014**, *43*, 14–32. [\[CrossRef\]](#)
- Lu, L.; Qin, J.-M.; Teng, B.; Li, Y.-C. Numerical investigations of lift suppression by feedback rotary oscillation of circular cylinder at low Reynolds number. *Phys. Fluids* **2011**, *23*, 033601.
- Dehkordi, B.G.; Jafari, H.H. On the suppression of vortex shedding from circular cylinders using detached short splitter-plates. *J. Fluids Eng.* **2010**, *132*, 044501. [\[CrossRef\]](#)
- Akilli, H.; Karakus, C.; Akar, A.; Şahin, B.; Tumen, N.F.; Akar, M. Control of vortex shedding of circular cylinder in shallow water flow using an attached splitter plate. *J. Fluids Eng.* **2008**, *130*, 041401. [\[CrossRef\]](#)
- Firat, E.; Akansu, Y.E.; Akilli, H. Flow past a square prism with an upstream control rod at incidence to uniform stream. *Ocean Eng.* **2015**, *108*, 504–518. [\[CrossRef\]](#)
- Seo, S.-H.; Nam, C.-D.; Han, J.-Y.; Hong, C.-H. Drag reduction of a bluff body by grooves laid out by design of experiment. *J. Fluids Eng.* **2013**, *135*, 111202. [\[CrossRef\]](#)
- Zhou, B.; Wang, X.; Guo, W.; Gho, W.M.; Tan, S.K. Control of flow past a dimpled circular cylinder. *Exp. Therm. Fluid Sci.* **2015**, *69*, 19–26. [\[CrossRef\]](#)
- Mishra, A.; Hanzla, M.; De, A. Passive control of the onset of vortex shedding in flow past a circular cylinder using slit. *Phys. Fluids* **2020**, *32*, 013602. [\[CrossRef\]](#)
- Strykowski, P.J.; Sreenivasan, K.R. On the formation and suppression of vortex ‘shedding’ at low Reynolds numbers. *J. Fluid Mech.* **1990**, *218*, 71–107. [\[CrossRef\]](#)
- Schulmeister, J.C.; Dahl, J.M.; Weymouth, G.D.; Triantafyllou, M.S. Flow control with rotating cylinders. *J. Fluid Mech.* **2017**, *825*, 743–763. [\[CrossRef\]](#)

13. Rashidi, S.; Hayatdavoodi, M.; Esfahani, J.A. Vortex shedding suppression and wake control: A review. *Ocean Eng.* **2016**, *126*, 57–80. [[CrossRef](#)]
14. Igarashi, T. Drag reduction of a square prism by flow control using a small rod. *J. Wind Eng. Ind. Aerodyn.* **1997**, *69*, 141–153. [[CrossRef](#)]
15. Yen, S.C.; Wu, S.F. Square-cylinder flow characteristics modulated using upstream control rod. *J. Mech.* **2012**, *28*, 279–289. [[CrossRef](#)]
16. Gim, O.-S.; Kim, S.-H.; Lee, G.-W. Flow control behind a circular cylinder by control rods in uniform stream. *Ocean Eng.* **2011**, *38*, 2171–2184. [[CrossRef](#)]
17. Chauhan, M.K.; Dutta, S.; Gandhi, B.K. Wake flow modification behind a square cylinder using control rods. *J. Wind Eng. Ind. Aerodyn.* **2018**, *184*, 342–361. [[CrossRef](#)]
18. Lu, L.; Liu, M.-M.; Teng, B.; Cui, Z.-D.; Tang, G.-Q.; Zhao, M.; Cheng, L. Numerical investigation of fluid flow past circular cylinder with multiple control rods at low Reynolds number. *J. Fluids Struct.* **2014**, *48*, 235–259. [[CrossRef](#)]
19. Silva-Ortega, M.; Assi, G. Hydrodynamic loads on a circular cylinder surrounded by two, four and eight wake-control cylinders. *Ocean Eng.* **2018**, *153*, 345–352. [[CrossRef](#)]
20. Silva-Ortega, M.; Assi, G. Suppression of the vortex-induced vibration of a circular cylinder surrounded by eight rotating wake-control cylinders. *J. Fluids Struct.* **2017**, *74*, 401–412. [[CrossRef](#)]
21. Mittal, S. Control of flow past bluff bodies using rotating control cylinders. *J. Fluids Struct.* **2001**, *15*, 291–326. [[CrossRef](#)]
22. Goodarzi, M.; Dehkordi, E.K. Geometrical parameter analysis on stabilizing the flow regime over a circular cylinder using two small rotating controllers. *Comput. Fluids* **2017**, *145*, 129–140. [[CrossRef](#)]
23. Goodarzi, M.; Dehkordi, E.K. Complete vortex shedding suppression allocating twin rotating controllers at a suitable position. *Ocean Eng.* **2017**, *137*, 215–223. [[CrossRef](#)]
24. Zhu, H.; Yao, J.; Ma, Y.; Zhao, H.; Tang, Y. Simultaneous CFD evaluation of VIV suppression using smaller control cylinders. *J. Fluids Struct.* **2015**, *57*, 66–80. [[CrossRef](#)]
25. Zhu, H.; Gao, Y. Vortex-induced vibration suppression of a main circular cylinder with two rotating control rods in its near wake: Effect of the rotation direction. *J. Fluids Struct.* **2017**, *74*, 469–491. [[CrossRef](#)]
26. Du, L.; Sun, X. Suppression of vortex-induced vibration using the rotary oscillation of a cylinder. *Phys. Fluids* **2015**, *27*, 023603. [[CrossRef](#)]
27. Williamson, C.H.K. Vortex dynamics in the cylinder wake. *Annu. Rev. Fluid Mech.* **1996**, *28*, 477–539. [[CrossRef](#)]
28. Zhao, M.; Thapa, J.; Cheng, L.; Zhou, T. Three-dimensional transition of vortex shedding flow around a circular cylinder at right and oblique attacks. *Phys. Fluids* **2013**, *25*, 014105. [[CrossRef](#)]
29. Zhao, M.; Cheng, L.; Teng, B.; Dong, G. Hydrodynamic forces on dual cylinders of different diameters in steady currents. *J. Fluids Struct.* **2006**, *23*, 59–83. [[CrossRef](#)]
30. Behr, M.; Hastreiter, D.; Mittal, S.; Tezduyar, T. Incompressible flow past a circular cylinder: Dependence of the computed flow field on the location of the lateral boundaries. *Comput. Methods Appl. Mech. Eng.* **1995**, *123*, 309–316. [[CrossRef](#)]
31. Song, B.; Ping, H.; Zhu, H.; Zhou, D.; Bao, Y.; Cao, Y.; Han, Z. Direct numerical simulation of flow over a cylinder immersed in the grid-generated turbulence. *Phys. Fluids* **2022**, *34*, 015109. [[CrossRef](#)]
32. Guo, F.; Wu, G.; Du, X.; Mason, M.S. Numerical investigation of flow around a square cylinder in accelerated flow. *Phys. Fluids* **2021**, *33*, 104105. [[CrossRef](#)]
33. Zhao, M. Flow induced vibration of two rigidly coupled circular cylinders in tandem and side-by-side arrangements at a low Reynolds number of 150. *Phys. Fluids* **2013**, *25*, 123601. [[CrossRef](#)]
34. Zhao, M.; Cheng, L.; Lu, L. Vortex induced vibrations of a rotating circular cylinder at low Reynolds number. *Phys. Fluids* **2014**, *26*, 073602. [[CrossRef](#)]
35. Assi, G.; Orselli, R.; Silva-Ortega, M. Control of vortex shedding from a circular cylinder surrounded by eight rotating wake-control cylinders at  $Re = 100$ . *J. Fluids Struct.* **2019**, *89*, 13–24. [[CrossRef](#)]
36. Soti, A.K.; Thompson, M.C.; Sheridan, J.; Bhardwaj, R. Harnessing electrical power from vortex-induced vibration of a circular cylinder. *J. Fluids Struct.* **2017**, *70*, 360–373. [[CrossRef](#)]